PALADYN Journal of Behavioral Robotics

VERSITA

Research Article · DOI: 10.2478/pjbr-2013-0019 JBR · 4(4) · 2013 · 211-222

Profile Following for Inspection of Underwater Structures

Enric Galceran*, **Narcís Palomeras**†, **Marc Carreras**‡

Underwater Robotics Research Center, University of Girona, Parc Científic i Tecnológic de la Universitat de Girona, Pic de Peguera, 13 17071 Girona, Catalonia, Spain

Received 30-04-2013

Accepted 16-12-2013

Abstract

We present a seabed profile estimation and following method for close proximity inspection of 3D underwater structures using autonomous underwater vehicles (AUVs). The presented method is used to determine a path allowing the AUV to pass its sensors over all points of the target structure, which is known as coverage path planning. Our profile following method goes beyond traditional seabed following at a safe altitude and exploits hovering capabilities of recent AUV developments. A range sonar is used to incrementally construct a local probabilistic map representation of the environment and estimates of the local profile are obtained via linear regression. Two behavior-based controllers use these estimates to perform horizontal and vertical profile following. We build upon these tools to address coverage path planning for 3D underwater structures using a (potentially inaccurate) prior map and following cross-section profiles of the target structure. The feasibility of the proposed method is demonstrated using the GIRONA 500 AUV both in simulation using synthetic and real-world bathymetric data and in pool trials.

Keywords

Autonomous underwater vehicles · sensor-based planning · seabed profile following · coverage path planning · behavior-based control

1. Introduction

Thanks to technology breakthroughs in the last two decades, surveys conducted by AUVs have become a standard tool supporting many marine robotics applications, such as marine geology [1, 2], underwater archaeology [3], habitat monitoring [4] and mine countermeasures (MCM) [5]. AUVs provide high resolution data thanks to near-bottom surveys and require little human supervision compared to their ship- or remotely operated vehicle (ROV)-assisted counterparts, and hence at a lower cost.

In most AUV survey missions conducted nowadays the vehicle follows a pre-planned survey path and keeps a constant, safe altitude from the sea bottom. A reactive obstacle avoidance controller is often used to maintain altitude. Typically, such controller takes measurements from a single altimeter. As a result, the controller is unable to anticipate the forthcoming terrain and needs to keep a conservative distance from the bottom. This is a serious limitation for a number of emerging applications requiring fine-scale seafloor surveys in close proximity enabling acquisition of high-resolution imagery or even object grasping. Examples include monitoring of cold water coral reefs, oil and gas pipeline inspection, harbor and dam protection and object recovery. Therefore, techniques able to navigate in closer proximity to the seabed without compromising vehicle safety are desired.

On the other hand, following the elevation profile of the seabed is a valid strategy when surveying effectively planar regions, but it does not provide satisfactory results when surveying intrinsically 3-dimensional, complex structures such as coral reefs, ship wrecks or protruding hydrothermal vents. These structures present very steep slopes that cannot be imaged with acceptable quality from an overhead viewpoint. As illustrated in Figure 1, a survey at a safe altitude from the bottom provides an askew sensor angle of incidence with respect to the bottom normal, resulting in poor imaging. In contrast, an angle of incidence parallel to the bottom normal is desired in applications requiring imaging.

These concerns can be addressed in the context of coverage path planning, which is the task of planning a path that allows a robot to pass its sensors over all points in a target area while avoiding obstacles. A considerable body of research has addressed the coverage path planning problem (see Section 2). A popular approach for coverage of 3-dimensional structures is to follow the cross-section profiles of the target structure at an offset distance. A strength of this approach is that the resulting path is predictable and enables acquisition of a clear and continuous dataset, simplifying the tasks of post-processing and analysis for both humans and automated procedures. However, in most prior work the coverage path is planned off-line using an *a priori* map and then it is assumed that the vehicle will perfectly follow the planned path. This is an unrealistic assumption due to the uncertainties in the *a priori* map and in the robot's sensing and control system. One way to deal with this uncertainties is to use advanced localization and control techniques such as simultaneous localization and mapping (SLAM) and stochastic control, requiring complex sensors and onboard processing capabilities. On the other hand, a simple range-sensing sonar can be used to perceive the target structure *in situ* and reactively follow its profiles to achieve coverage.

Toward this aim, we propose in this work a profile estimation and following method able to provide close proximity, fine-scale coverage of underwater structures using a range-sensing sonar. Our profile estima-

*E-mail: enricgalceran@eia.udg.edu
†E-mail: npalomer@eia.udg.edu
‡E-mail: marc.carreras@udg.edu

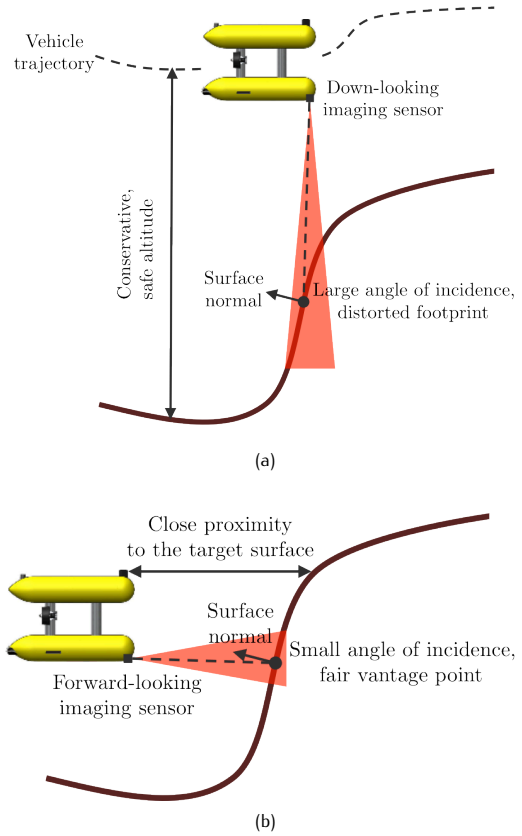

Figure 1. Askew sensor angle of incidence provided by a constant, safe altitude survey (a) in contrast to the small angle of incidence (b) obtained by imaging the surface in parallel to its normal.

tion and following method handles both vertical and horizontal seabed profiles and does not require *a priori* knowledge of the terrain. A probabilistic local map of the immediate AUV surroundings is built and maintained onboard the vehicle using sonar range information. The probabilistic representation accounts for noisy measurements while allowing to estimate the profile using previously sensed ranges as new data becomes available. Estimates of the local profile to follow are obtained by means of simple linear regression on certain regions of interest of the map around the vehicle. To perform profile following using these estimates, behavior-based horizontal and vertical profile following controllers are provided. These controllers exploit hovering capabilities of recent AUV developments and are able to maneuver the vehicle surveying the target structure in close proximity while avoiding collision. We then show how this profile estimation and following framework can be used as part of a coverage path planning scheme for inspection tasks to achieve coverage of a 3-dimensional underwater structure by following cross-section profiles of the structure at incremental depths. The feasibility of the proposed methods is demonstrated both in simulation and in pool trials using GIRONA 500, a hovering-capable AUV.

The remainder of this paper is organized as follows. Section 2 briefly reviews related work in seabed following and coverage path planning reported in the literature. Sections 3 and 4 introduce our proposed strategy for profile estimation and following. Section 5 describes how a coverage path planning task can be achieved using our proposed profile estimation and following strategy. Section 6 introduces GIRONA 500, the AUV we use to demonstrate our method, and experimental results are reported in Section 7. Lastly, concluding remarks and directions for further research are given in Section 8.

2. Related work

The bottom following problem, described as "maintaining a fixed altitude above an arbitrary surface whose characteristics may or may not be known" [6], has been addressed in many research works using different sensors, such as high-frequency pencil-beam profiling sonars [7] or a pair of altimeters to estimate the profile [8]. In regard to AUV control, a variety of different schemes have been proposed for bottom following. Creuze *et al.* proposed a seabed-following trajectory generation algorithm for torpedo-shaped vehicles [9]. Their algorithm computes trajectories using simple geometric functions and interpolation curves called "semi-forced cubic splines." Melo and Matos presented a basic guidance approach to provide depth and pitch references to, as in the aforementioned work, a torpedo-shaped vehicle [10]. Other works propose more complex control techniques such as nonlinear output regulation [11]. Recently, Houts *et al.* presented a technique for aggressive seabed terrain following [12]. Estimates from a terrain-based navigation system are used to anticipate the terrain. As in this work, their method pursues closer proximity seabed following. However, their technique is concerned only with the seabed's vertical profile. Karras *et al.* proposed a robust control scheme for wall profile (horizontal) following using sonar measurements [13].

As described, in this work we show how to use horizontal profile following to achieve coverage of a complex structure on the seabed, tackling the coverage path planning problem. A large body of research has investigated coverage path planning in 2D [14, 15], 2.5D [16–18] and 3D [19, 20] environments. Applications of coverage path planning in domains such as agricultural robotics [21] and unmanned aerial vehicles (UAVs) [22, 23] have been reported in the literature. However, while many underwater robotics applications, such as microbathymetry mapping, habitat monitoring or image photomosaicing, can benefit greatly from the complete coverage guarantees and robustness of coverage path planning methods, their application to underwater environments up to date has been limited. Especially, research on 3D path planning for underwater vehicles so far often only deals with abstract scenarios based on very simple simulations. Examples include sets of randomly placed spheres of different sizes [24] and randomly occupied cells in a grid [25]. Notable exceptions are the recent work in coverage path planning for ship hull inspection tasks presented in [26] and the 6 DOF 3D path planning approach presented in [27]. In general, however, few research has studied coverage path planning in the underwater domain. The strategy of following cross-sections of the target surface we use for coverage is particularly related to the algorithm by Atkar and Choset [19]. Nonetheless, that algorithm deals with an idealized scenario with perfect sensing and requires a full $360°$ range sensor ring.

3. Profile estimation

Our profile estimation method is targeted at AUVs equipped with a pencil-beam sonar or a sonar array providing range information in a circular sector of $180°$. Although we focus on AUVs equipped with sonar in this article, the same strategy we propose can be used with

other range-and-bearing sensors, such as stereo cameras. We use a two-module profile estimation process. First, a mapping module uses the sonar range information to construct and maintain a local map of the profile to follow. Second, a profile estimation module performs linear regression on certain regions of the local map to obtain an estimate of the profile around the vehicle.

3.1. Local Mapping

We use the sonar range information to construct and maintain a local, probabilistic occupancy-grid map of the structure profile to follow. The probabilistic map serves two main purposes. First, it allows to deal with noisy measurements by assigning a higher likelihood to cells that have been consistently reobserved as either occupied or free and hence filtering out outliers. Second, it provides a convenient representation upon which to perform profile estimation at a higher rate than the sensed ranges arrival rate (the later being typically slow in the case of mechanically scanning devices).

In fact, depending on configuration settings, mechanically scanning pencil-beam sonars take up to several seconds to provide a scan. It is the case of the pencil-beam sonar we use in our experiments (see Section 7 below), which takes up to 4 seconds to provide a $180°$ scan. Waiting for a whole sector scan to become available delays the subsequent profile estimation process on the recently collected sonar beams. We tackle this problem by feeding subsequent small sub-sector scans (of about $10°$, depending on configuration) to the mapping framework. By doing so we obtain more frequent map updates, enabling the profile estimation module to promptly incorporate recent sonar readings. To correct the distortion induced by the vehicle motion, we use the vehicle position estimates obtained during the scan time.

It is worth noting that, even if using a fast sensor (such as a multibeam sonar or a stereo camera) to perceive the profile, the probabilistic map representation is still beneficial in dealing with noisy measurements and obtaining a reliable perception as the environment is reobserved.

We use the Octomap [28] probabilistic mapping framework to construct and maintain our 3D map, which uses an octree map compression method to keep the 3D model compact and quickly accessible. Figure 2 shows a snapshot of a local map constructed in our laboratory's pool.

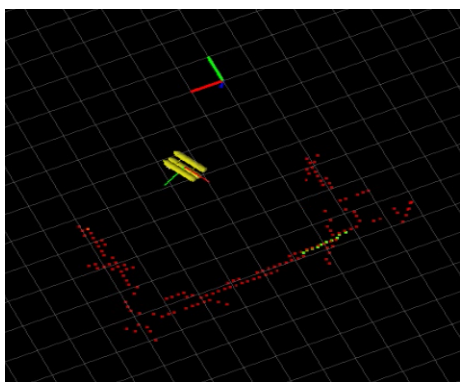

Figure 2. Local mapping module running on our laboratory's pool. The lightest (green) points show the latest incorporated sonar sub-scan and the red points show the occupied cells (with probability > 0.5) in the map. A real-sized model of our AUV (see Section 6) and the world and vehicle coordinate frames are also shown.

3.2. Profile Estimation on Regions of Interest

The profile estimation module operates on different regions of interest on the map, providing a local profile estimation for each region. Then, these estimates are appropriately used by the profile following modules. The horizontal profile estimation module operates on two regions, one in the front of the vehicle and one on the right of the vehicle, as depicted in Figure 3.

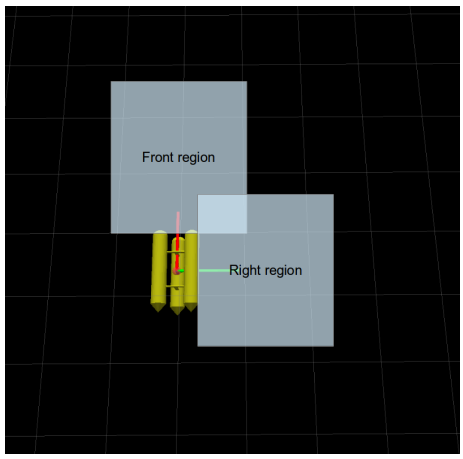

Figure 3. Regions of interest for horizontal profile estimation.

The vertical profile estimation module operates on the three regions shown in Figure 4: one below the vehicle, termed "bottom region"; one in front of the vehicle, termed "cliff region"; and one above the vehicle, termed "ceiling region".

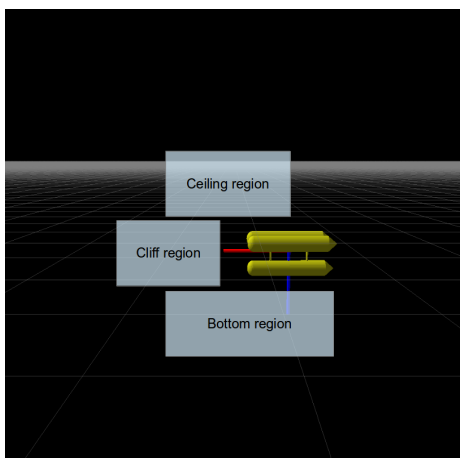

Figure 4. Regions of interest for vertical profile estimation.

The size of these regions is determined by the size of the vehicle and by the desired offset distance at which the profile needs to be followed. The 3D coordinates of the occupied cells (with probability > 0.5) of the map are projected on a 2D horizontal or vertical plane depending

on the current profile following mode. Then the profile is estimated on the 2D projection.
We estimate the local profile on each projected map region of interest by fitting a line to the points in the region. A line $y = ax + b$ is fitted to the N points (x_i, y_i) in the region via least squares, with slope a and intercept b given as follows:

$$a = \frac{\sum y_i - b \sum x_i}{N},$$

$$b = \frac{N \sum (x_i y_i) - (\sum x_i)(\sum y_i)}{N \sum x_i^2 - (\sum x)^2}.$$

More complex interpolation methods, such as splines [29], could be used for profile estimation. These techniques could be beneficial when the AUV is following a profile from far enough so it perceives a large piece (in the order of several meters) of the profile after one sensor scan. However, our target application (inspection of underwater structures) requires following the profile in close proximity, and therefore only a small piece of the profile is visible to the vehicle at any given time. In this situation the profile can be effectively approximated as a straight line. Moreover, line fitting can be computed quickly and provides a compact two-parameter representation.
Additionally, we compute the average distance from the points to the vehicle's reference frame, $\hat{d}$. Figure 5 shows the profile estimation procedure operating on a 3D structure in a simulated environment.

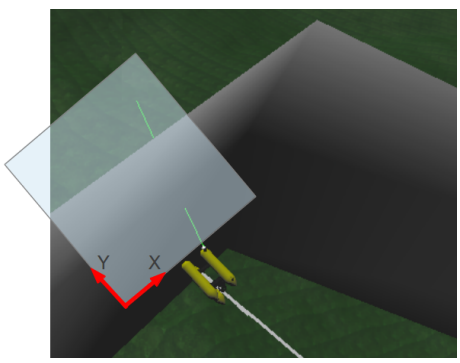

(a) Simulated environment.

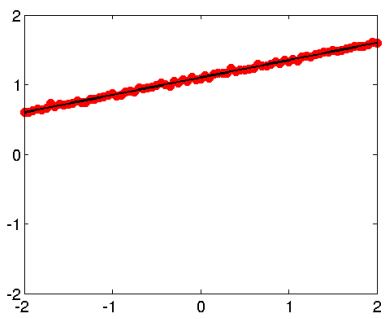

(b) X-Y plot showing the plane-projected map points and the estimated line corresponding to the scene shown in (a).

Figure 5. Profile estimation.

4. Profile following

We have designed and implemented two profile following modules, one for horizontal profile following and one for vertical profile following. It is assumed that the vehicle is hovering-capable and can be controlled in the surge (X), sway (Y), heave (Z) and heading (yaw) degrees of freedom (DOFs), although controllability in sway is not required for vertical profile following. The modules use the output from profile estimation and are designed as a set of coordinated behaviors which use proportional-integral (PI) controllers to generate speed commands in the appropriate DOFs. The speed commands generated by the behaviors are not sent directly to the vehicle's thrusters, but rather sent to a low-level velocity controller which merges and coordinates all the commands sent from all the modules of the robot's control architecture (see Section 6.1 for further details).

4.1. Horizontal Profile Following

The horizontal profile following module consists of a single behavior operating on the surge (X), sway (Y) and heading (yaw) DOFs. It assumes that an external module controls the vehicle to keep a certain constant depth.
The module seeks to advance the vehicle along the frontal region profile while keeping a certain desired distance, δ_h, from the frontal profile and facing perpendicularly to the profile (that is, keeping the profile slope, a, close to 0). The vehicle is advanced along the profile counter-clockwise (from an overhead viewpoint).
As shown in Figure 6, a PI controller operating on the X DOF is fed the frontal distance error, $e_{hf} = \delta_h - \hat{d}$, which it seeks to keep to 0. A second PI controller on the heave DOF is fed the slope, a. When both e_{hf} and a are below user-provided tolerances, the vehicle advances in the Y DOF at constant speed, V_y. Together with V_y, the desired speeds in the X and yaw DOFs (V_x and V_{yaw}, respectively) are sent as setpoints to the vehicle's low-level velocity controller.

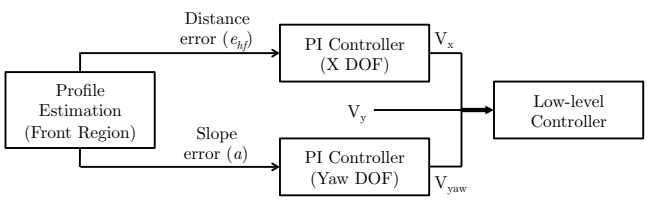

Figure 6. Horizontal profile following block diagram.

The module keeps track of the average distance to the profile in the right region. If a profile is detected on the right region and the distance to that profile is less than δ_h, it turns the robot 90° clockwise. This effectively moves the front region to where the right region was located, allowing the robot to successfully react to highly non-convex profiles. Indeed, using this strategy avoids performing profile estimation in regions where a linear fit is difficult to be reliably maintained (such a sharp "V" in the profile). After the 90° turn, the profile following continues. This procedure is illustrated in Figure 7.
Very acute corners on the profile are seen by the profile estimation module as discontinuities. In practice, that means that the profile vanishes in presence of such corners, from the point of view of the robot's perception. In case that, during profile following, the profile estimation module fails to detect the profile, the module steers the vehicle to trace a circular trajectory with radius equal to δ_h (the vehicle's surge axis facing

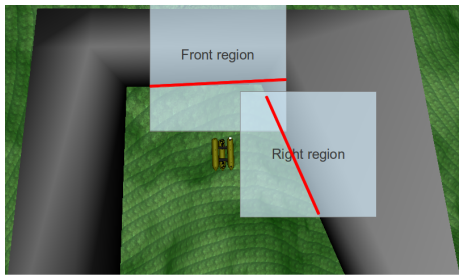

(a)

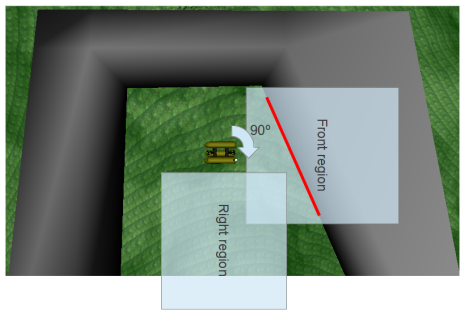

(b)

Figure 7. 90° turn maneuver on detection of a profile in the right region when performing horizontal profile following.

always its center). The robot traces the trajectory for a minimum sector angle (provided as a parameter), ignoring any potential profile estimation information. Then, it continues tracing the circular trajectory until the profile is detected. This allows the robot to continue profile following on the presence of very acute angles. This profile recovery maneuver is illustrated in Figure 8.

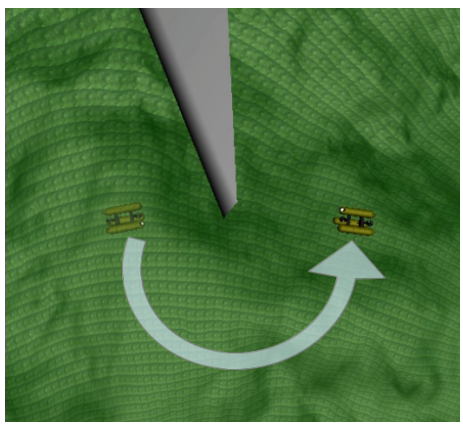

Figure 8. Horizontal profile recovery maneuver.

4.2. Vertical Profile Following

The vertical profile following module is implemented as a set of three coordinated behaviors: bottom following, cliff following and ceiling following. It is assumed that the robot is kept heading at a constant angle by an external module during vertical profile following.

A multiplexor selects which of the three behaviors takes over according to the profile estimation, that is, it enables the behavior for which a profile is detected in its associated region. If more than one behavior meets the condition, the behavior with the most recent associated profile estimation takes over. PI controllers in the X and Z DOFs are used by each behavior to keep the robot at a constant average distance, δ_v, from the profile (that is, they seek to keep $\delta_v - \hat{d} = 0$). Figure 9 shows a diagram of the vertical profile following module.

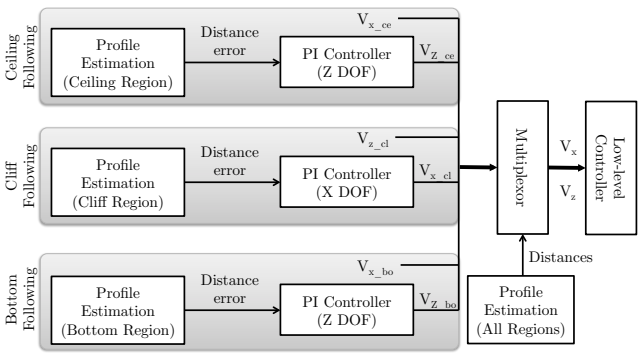

Figure 9. Vertical profile following block diagram.

To avoid steering the vehicle backwards in the surge axis, the ceiling following behavior makes the vehicle turn 180° in yaw when it is engaged. Then, it proceeds steering the vehicle forward and keeping the appropriate distance from the ceiling. When the behavior is disengaged, it reverts the initial turn. This procedure allows the robot to surge forward in a direction well suited for its hydrodynamic configuration.

5. 3D coverage using profile following

Next, we build upon our profile estimation and following framework to achieve coverage of 3-dimensional underwater structures for inspection tasks. The strategy we use consists in performing horizontal profile following on the cross-section profiles of the target structure at incremental depths. By adhering to this strategy, the vehicle is able to image the structure with a smaller angle of incidence than from the overhead viewpoint provided by traditional bottom following.

Our coverage path planning approach is a two-phase process. First, we use an *a priori* bathymetric map* (typically of low resolution) to determine a coverage plan consisting of the inter-profile spacing, the number of cross-section profiles to be followed and the order in which

* It is common in marine robotics applications to have prior knowledge of the target area in the form of low resolution bathymetry (i.e., an elevation map of the sea floor). The objective of an inspection mission is usually to obtain a more refined data product.

they will be followed. The strategy we use to generate this coverage plan is based in our prior work in coverage path planning presented in [30]. Next, we execute profile following on-line on each determined cross-section profile of the target structure using the scheme presented in Sections 3 and 4.
It is worth noticing that, while a coverage path can be fully determined offline using the *a priori* map [30], relying on an idealized, successful execution of such path is not a reasonable assumption due to sensing and control error on the AUV and to inaccuracies on the map. By contrast, using reactive profile following behaviors to inspect the target structure allows to adapt to the actual terrain *in situ* and deal with these uncertainties.

5.1. Off-line Coverage Planning Phase

To decide the cross-section profiles that the AUV must follow to achieve complete coverage of the structure we take the *a priori* bathymetric map and intersect it with horizontal planes at depths $\lambda_1, \lambda_2, \ldots, \lambda_N$. The horizontal planes are uniformly spaced along the vertical dimension, with their spacing $\Delta\lambda$ being determined by the desired offset distance Ω and the aperture angle of the imaging sensor at use, α, as shown in Figure 10.

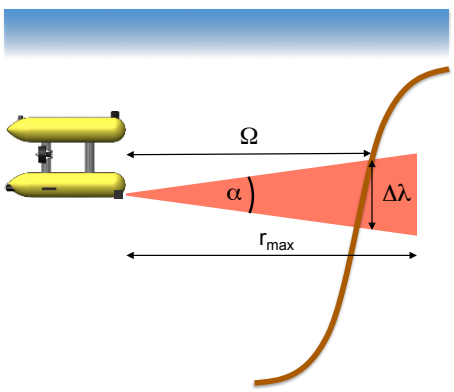

Figure 10. The robot's sensor aperture angle α and offset distance Ω determine the sensor footprint on the target surface. The sensor footprint, determines the distance between the horizontal planes, $\Delta\lambda$, used to determine the cross-section profiles to follow.

For each horizontal plane λ_i, we obtain M intersection edges $e_{\lambda_i,1}, e_{\lambda_i,2}, \ldots, e_{\lambda_i,M}$. A starting point where the robot will initiate horizontal profile following is assigned to each intersection edge. The robot can safely move from one starting point to the next in a straight line, given that the starting point on the next edge is chosen to be the closest to the previous starting point. This off-line planning process is illustrated in Figure 11.

5.2. On-line Profile Following Phase

Once the cross-section profiles to be covered and their starting points have been determined, we proceed to inspect them using our profile estimation and following method on-line.
Initially, the AUV approaches the first starting point by diving towards it from the surface. Then, the horizontal profile following behavior is engaged and the inspection begins. The vehicle's onboard navigation system is used to estimate its trajectory and determine when a complete cross-section profile loop has been completed. When a loop is

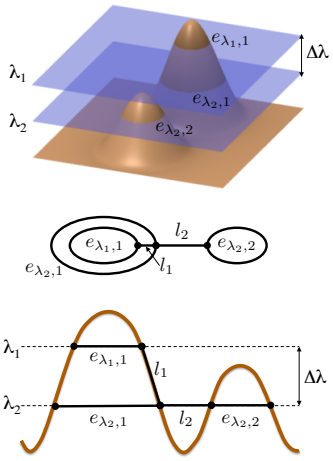

Figure 11. 3D view (top), top view (middle) and side view (bottom) of the horizontal plane intersection process applied at two different depth levels (λ_1, λ_2) on an example *a priori* map. At level λ_1, the intersection comprises one single edge, $e_{\lambda_1,1}$. At λ_2, the intersection comprises two edges, $e_{\lambda_2,1}$ and $e_{\lambda_2,2}$. Straight lines l_1, l_2 represent the vehicle motions from one starting point to the next.

completed, the vehicle approaches the starting point of the next profile and repeats the profile following process until all profiles determined in the off-line planning phase have been covered.

6. The Girona 500 AUV

We have tested our method using the GIRONA 500 AUV [31], a reconfigurable vehicle rated for depths up to 500 m shown in Figure 12.

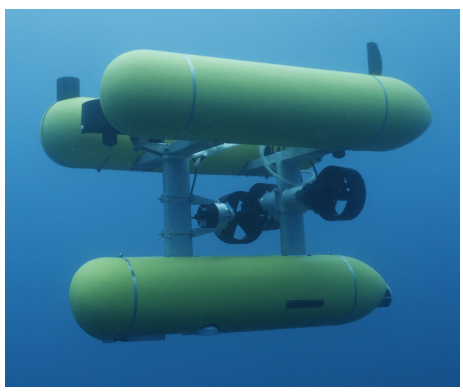

Figure 12. The GIRONA 500 AUV with the SeaKing pencil-beam sonar protruding on the top-left.

GIRONA 500 is a hovering-capable AUV actuated in 4 DOFs: surge, sway, heave and yaw. The two upper hulls, which contain the flotation foam and the electronics housing, are positively buoyant, while the

lower one contains the more heavy elements such as the batteries and the payload. Thanks to this arrangement, GIRONA 500 is passively stable in roll and pitch. The overall dimensions of the vehicle are 1 m height, 1 m width, 1.5 m length, weighing less than 200 Kg. It is equipped with a sensor suite including a SeaKing pencil-beam sonar from Tritech, which we use to estimate the underwater structure profile in the vertical or the horizontal plane of the robot. A rotary support makes it easy to orientate the sonar to scan in the horizontal or the vertical plane. Apart from the pencil-beam sonar, GIRONA 500 is equipped with a navigation sensor suite including a GPS for positioning while at the surface, an attitude and heading reference system (AHRS) and a Doppler velocity log (DVL).

6.1. COLA2: GIRONA 500's Control Architecture

GIRONA 500 is driven by a control architecture termed COLA2 (Component-Oriented Layer-based Architecture for Autonomy) [32], developed at our lab. A simplified diagram of COLA2 highlighting its components involved in profile following for inspection tasks is shown in Figure 13. To address an inspection task, the off-line coverage planning module first generates a coverage plan using a prior map, as described in Section 5. The coverage plan is fed to the Task Execution component, which decides when to engage each profile following component according to the plan. The profile following components send commands to the low-level velocity controller, which then generates and sends velocity setpoints to the vehicle's thrusters. The navigation and mapping modules estimate the vehicle's trajectory and map its environment, respectively. These trajectory estimates and local maps are used by the profile estimation component to estimate the profile to be followed and feed it to the profile following components.

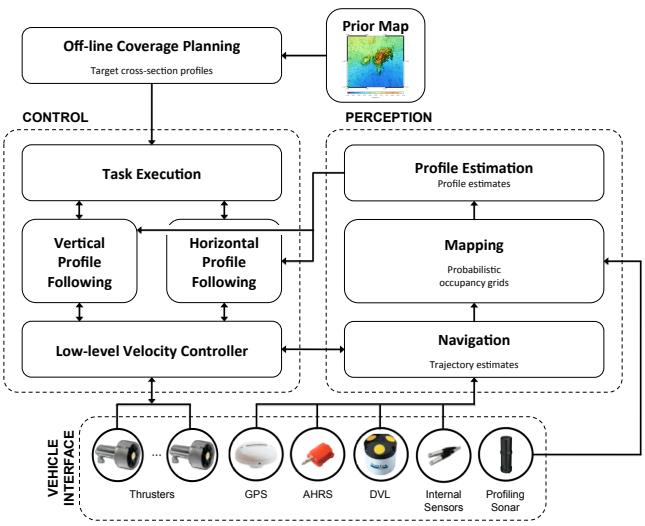

Figure 13. COLA2: GIRONA 500's control architecture for profile following and inspection tasks.

7. Results

Next, we show results of our profile following method obtained both in simulation and in pool trials with the GIRONA 500 AUV. First, we show results obtained in simulation of our vertical profile following scheme on a man-made object model. Next, we test our horizontal profile following scheme in a simulated 3D coverage task of a seamount. We use a model of a real-world seamount built from a bathymetric dataset autonomously recorded by GIRONA 500 in the target area. We finally report on two in-water trials conducted in our lab's pool, where GIRONA 500 follows the vertical and horizontal profiles of the pool.

For the simulation experiments we use the UWSim [33] underwater robotics simulation package, which provides a high-fidelity simulation environment. We import into UWSim a dynamic model of GIRONA 500 and a rotating pencil-beam sonar sensor model. The very same software architecture which runs on GIRONA 500 during sea trials is used in conjunction with UWSim to carry out the simulation, thus allowing for seamless transition from simulation to real-world missions.

7.1. Simulated Vertical Profile Following

Figure 14 shows the trajectory traced by GIRONA 500 when using the proposed method to follow the vertical profile of a man-made object model. The desired offset distance is 2 m. As can be observed in Figure 14, by exploiting the hovering capability of GIRONA 500 our profile following method is able to successfully maneuver the vehicle to completely follow the "C" profile of the object. Due to the presence of a totally vertical profile traditional bottom following techniques would not be able to handle it, leading to a collision threat for the vehicle. Our method favors hovering-capable AUVs, being able survey structures in closer proximity than traditional bottom following surveys typically used in torpedo-shaped vehicles. Note that the robot makes a 180° turn to avoid navigating backwards when the ceiling following behavior is engaged.

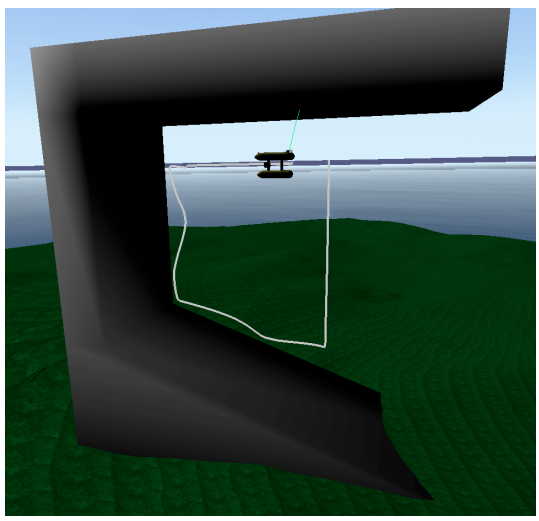

Figure 14. Trajectory traced by GIRONA 500 while following the vertical profile of a man-made object in simulation.

7.2. Simulated 3D Coverage using Profile Following using a Real-World Bathymetric Dataset

We now show results obtained in simulation using a bathymetric model of l'Amarrador seamount, a popular diving site off the Costa Brava in

Sant Feliu de Guíxols, Girona, Catalonia. The seamount rises from 40 m depth up to 28 m, being approximately 12 m high. The dataset was collected by GIRONA 500 following a pre-planned survey path with a multibeam sonar at 5 m depth in April 2013. The bathymetric chart of the site obtained from the data gathered during the survey mission is shown in Figure 15. Each cell in the uniform grid composing the bathymetric model is 40-by-40 cm. Figure 16 shows the 3D model of the site obtained from the bathymetry, which is imported into UWSim to perform the simulation.

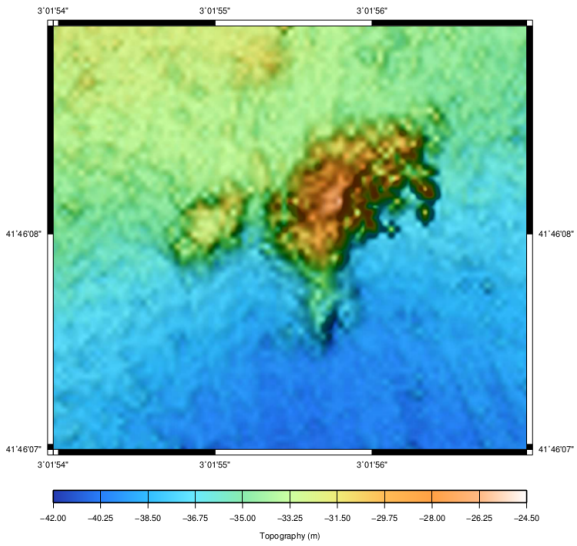

Figure 15. Bathymetric map of l'Amarrador site. Data were collected by GIRONA 500.

We automatically generate an off-line coverage plan for the task consisting of two cross-section profiles, the first at a constant 5 m depth below the summit of the seamount and the second at 3 m below the summit. This off-line coverage plan is illustrated in Figure 16 with the triangle mesh model of the site used in simulation. The desired offset distance is $\Omega = 5$ m, and it is assumed that the vehicle is using a payload sensor with a $60°$ field-of-view, such as a typical camera.

The trajectory traced by GIRONA 500 during the profile-following-based coverage experiment is shown Figure 17 and Figure 18 shows the distance and slope errors during profile following in the diving site. The trajectory presents some sharp features induced by the low resolution and roughness of the 3D model of the seamount used in the simulation. For this very same reason, the method eventually needs a few seconds to deal with a highly non-convex region of the profile. This situation arose around the second 450 in our experiment (see Figure 18), where a high-frequency period of approximately 20 seconds takes place until the method is able to successfully detect a profile to the right of the vehicle and perform the $90°$ turn maneuver described in Section 4.1. We hypothesize that in the real-world site this situation is less likely to happen since the actual profile of the seamount is smoother than that of the 3D model used in the simulation. Overall, this experiment shows how our method can successfully cover the target structure by following its complex profiles within 1.5 m of the nominal desired distance.

This experiment serves as a proof of concept of coverage of a protruding, rugged region of the seabed using our profile following method at

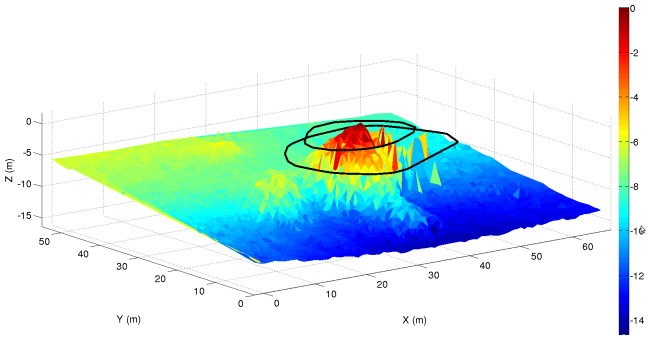

Figure 16. 3D triangle mesh model of l'Amarrador site with the off-line coverage plan consisting of 2 target cross-section profiles: one at 5 m below the summit and another at 3 m below the summit. The desired offset distance is $\Omega = 5$ m.

incremental depths. Indeed, by following the trajectory obtained with our method the AUV is able to image the target surface using a forward-looking sensor. Since the profile following method orientates the vehicle along the profile normal, an appropriate viewpoint for imaging purposes is obtained. This contrasts with the askew angle of incidence obtained from an overhead viewpoint using traditional bottom profile following.

7.3. In-Water Profile Following Trials

We tested our method in a real-world setting with the GIRONA 500 AUV following the vertical and horizontal profiles of our pool at the Underwater Robotics Research Center of the University of Girona. As shown in Figure 19, the pool has a "V" shaped bottom. A supervision room with a window under the water level allows to keep track of the AUV operation.

We tested the horizontal profile following module at a constant 4 m depth. Figure 20 shows a sequence of photos of GIRONA 500 following the horizontal profile of the pool, seen from the supervision room.

The frontal distance and slope errors of two complete circumnavigations of the pool's horizontal profile are shown in Figure 21. Despite the sharp $90°$ corners in the pool's profile, our profile following method is able to keep the estimated front distance within 1 m of the desired nominal distance.

The vertical profile following module was tested along the profile of the pool. Figure 22 shows the estimated frontal distance to the profile (in the cliff region) during the vertical profile following in the pool. The AUV started in the shallow region of the pool (left of Figure 19(b), moving to the right), where the pencil-beam sonar faced both the opposite ramp and the farthest wall of the pool. As a result, sonar energy returns from said ramp and wall lead to a spread occupied area on the local map and, consequently, to a poor estimation of the actual profile. Effectively, returns from the wall and from the ramp were being confused in the vehicle's perception. Due to this situation, a region of high error appears in Figure 22 during the first 20 seconds of the experiment. Once the vehicle reaches the first ramp on the pool's profile and the vehicle dives the sonar measurements start to match the actual environment and the vehicle can adjust its distance to the estimated profile. For the same reason, at second 40 another error peak arises when the vehicle reaches the end of the second ramp. The error in this experiment could have been reduced by using a pencil-beam sonar with a narrower beam, providing a more accurate mapping of the profile. We note, how-

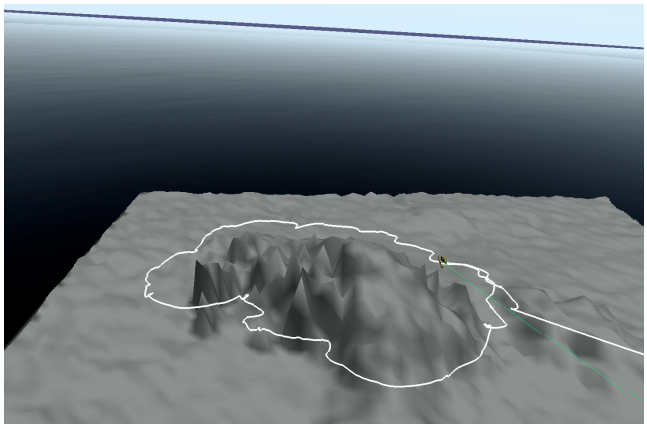

(a)

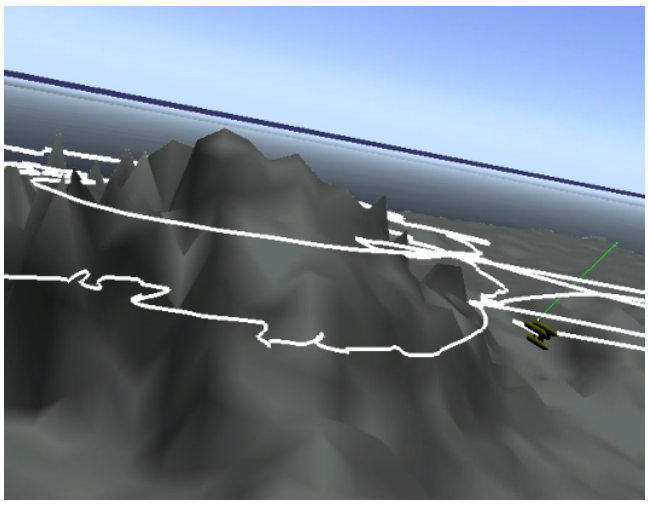

(b)

Figure 17. Path traced by GIRONA 500 when performing coverage of l'Amarrador site using horizontal profile following in simulation: path after following the deepest profile (a) and path after finishing following the second profile (b).

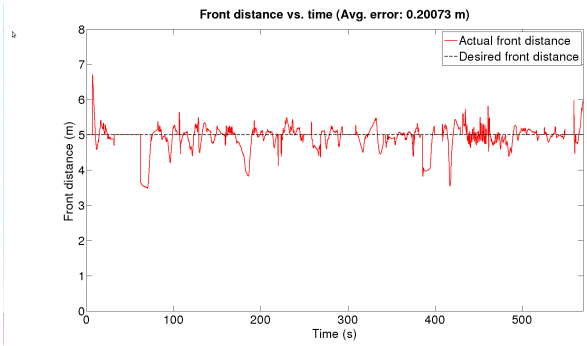

(a)

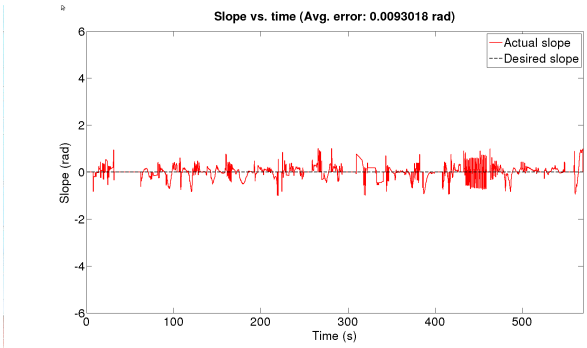

(b)

Figure 18. Simulated coverage using horizontal profile following at l'Amarrador site: frontal distance (a) and slope (b) given by our profile estimation process vs. time.

ever, that due to the relatively big size of GIRONA 500 in comparison with the profile followed and the non-convex and confined environment this was a challenging profile following task.

8. Conclusion

We have presented perception and navigation techniques for seabed profile estimation and following using hovering-capable AUVs. The proposed profile estimation technique uses a local map and simple linear regression to obtain an estimate of the profile in certain regions of interest around the robot. The probabilistic, occupancy-grid local map constructed using sonar range measurements provides a means to deal with noisy measurements by assigning a higher likelihood to regions of the environment that have been consistently reobserved. The profile estimation information is then used by behavior-based profile following modules which reactively guide the vehicle to follow the estimated profile. Our method is suited for both vertical and horizontal profile following, enabling inspection of seabed structures in close proximity. Moreover, we have shown how our profile following framework can be exploited to achieve coverage of complex, protruding 3D structures on the seabed. The method has been tested both in simulation and in-water trials using GIRONA 500, which have demonstrated the effectiveness of our approach. The method performed well both in structured (swimming pool) and unstructured (diving site) scenarios.

We will focus our immediate efforts on testing the profile estimation and following techniques here presented at sea, following natural structures of interest. We would like to study the use of multimodal sensing (e.g. stereo vision, multi-beam sonars, acoustic cameras) for constructing the local map. We believe this would lead to more accurate profile estimates, although at a higher computational cost. The current profile following control scheme we use can deal with inspection tasks where the vehicle moves at slow speeds. However, moving at higher speeds would require more responsive controllers and sensors providing measurements at a fast rate. Therefore, we are interested in exploring robust control techniques to increase the profile following accuracy of our method and improve its speed performance.

(a)

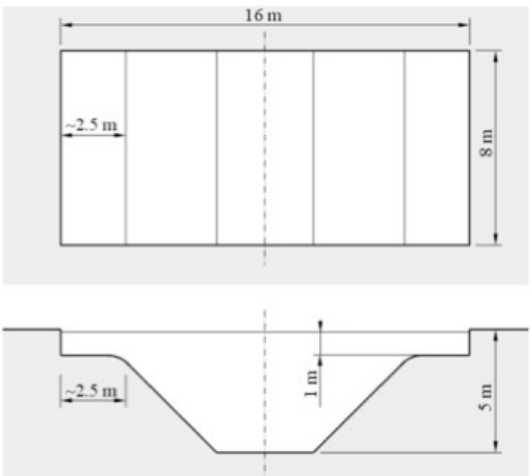

(b)

Figure 19. Premises of the Underwater Robotics Lab of the University of Girona (a) with a blueprint of its pool (b).

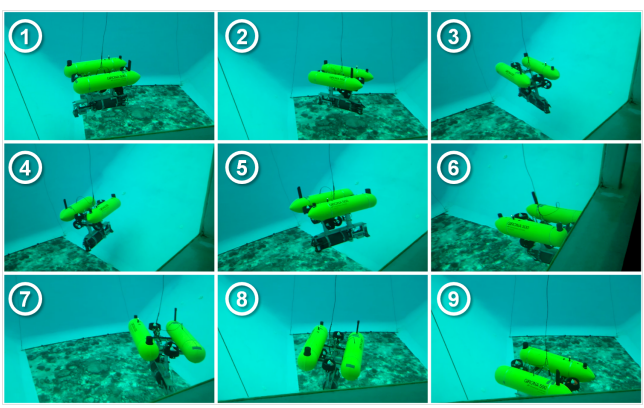

Figure 20. Photo sequence (left to right, top to bottom) of GIRONA 500 following the horizontal profile of our lab's pool.

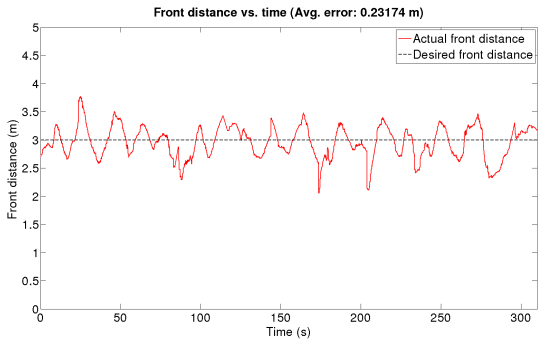

(a)

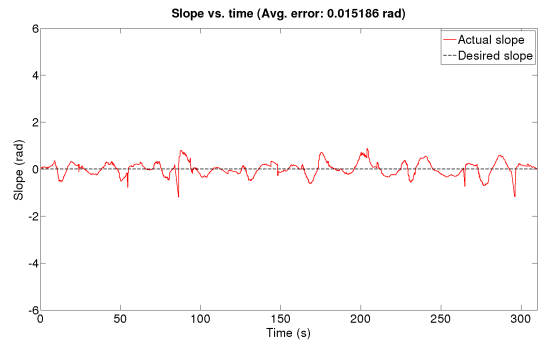

(b)

Figure 21. In-pool horizontal profile following: frontal distance (a) and slope (b) vs. time.

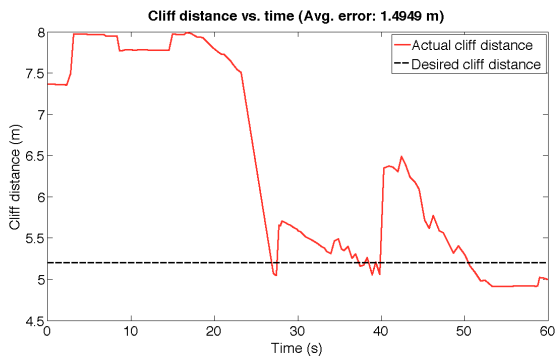

Figure 22. In-pool vertical profile following: distance to cliff (frontal wall) vs. time.

Acknowledgment

We are sincerely grateful to the anonymous reviewers for their valuable comments.

This research was sponsored by the Spanish government (COMAROB Project, DPI2011-27977-C03-02) and the MORPH EU FP7-Project un-

der the Grant agreement FP7-ICT-2011-7-288704. We are grateful for this support.

References

[1] J. Escartin, R. Garcia, O. Delaunoy, J. Ferrer, N. Gracias, A. Elibol, X. Cufi, L. Neumann, D. J. Fornari, S. E. Humphris, and J. Renard, "Globally aligned photomosaic of the lucky strike hydrothermal vent field (mid-atlantic ridge, 37 deg 18.5 min n): Release of georeferenced data, mosaic construction, and viewing software," *Geochemistry, Geophysics, Geosystems*, vol. 9, no. 12, pp. n/a–n/a, 2008. [Online]. Available: http://dx.doi.org/10.1029/2008GC002204

[2] D. R. Yoerger, D. S. Kelley, and J. R. Delaney, "Fine-scale three-dimensional mapping of a deep-sea hydrothermal vent site using the jason rov system," *The International Journal of Robotics Research*, vol. 19, no. 11, pp. 1000–1014, 2000. [Online]. Available: http://ijr.sagepub.com/content/19/11/1000.abstract

[3] B. Bingham, B. Foley, H. Singh, R. Camilli, K. Delaporta, R. Eustice, A. Mallios, D. Mindell, C. N. Roman, and D. Sakellariou, "Robotic tools for deep water archaeology: Surveying an ancient shipwreck with an autonomous underwater vehicle," *J. Field Robotics*, vol. 27, no. 6, pp. 702–717, 2010.

[4] P. Rigby, O. Pizarro, and S. B. Williams, "Toward adaptive benthic habitat mapping using gaussian process classification," *Journal of Field Robotics*, vol. 27, no. 6, pp. 741–758, 2010. [Online]. Available: http://dx.doi.org/10.1002/rob.20372

[5] D. P. Williams, "On optimal auv track-spacing for underwater mine detection," ICRA, pp. 4755–4762, 2010.

[6] A. Bennet, J. Leonard, and J. Bellingham, "Bottom following for survey-class autonomous underwater vehicles," in *International Symposium on Unmanned Untethered Submersible Technology*, 1995, pp. 327–336.

[7] M. Caccia, G. Bruzzone, and G. Veruggio, "Active sonar-based bottom-following for unmanned underwater vehicles," *Control Engineering Practice*, vol. 7, no. 4, pp. 459 – 468, 1999. [Online]. Available: http://www.sciencedirect.com/science/article/pii/S0967066198001683

[8] M. Caccia, R. Bono, G. Bruzzone, and G. Veruggio, "Bottom-following for remotely operated vehicles," *Control Engineering Practice*, vol. 11, no. 4, pp. 461 – 470, 2003. [Online]. Available: http://www.sciencedirect.com/science/article/pii/S0967066101001423

[9] V. Creuze, B. Jouvencel, and P. Baccou, "Seabed following for small autonomous underwater vehicles," in *OCEANS, 2001. MTS/IEEE Conference and Exhibition*, vol. 1, 2001, pp. 369 –374 vol.1.

[10] J. Melo and A. Matos, "Bottom estimation and following with the mares auv," in *Oceans, 2012*, oct. 2012, pp. 1 –8.

[11] A. Adhami-Mihosseini, A. Aguiar, and M. Yazdanpanah, "Seabed tracking of an autonomous underwater vehicle with nonlinear output regulation," in *Decision and Control and European Control Conference (CDC-ECC)*, 2011, pp. 3928 – 3933.

[12] S. Houts, S. Rock, and R. McEwen, "Aggressive terrain following for motion-constrained auvs," in *Autonomous Underwater Vehicles (AUV), 2012 IEEE/OES*, 2012, pp. 1–7.

[13] G. Karras, C. Bechlioulis, H. Abdella, T. Lakworthy, K. Kyriakopoulos, and D. Lane, "A robust sonar servo control scheme for wall-following using an autonomous underwater vehicle," in *Intelligent Robots and Systems (IROS)*, 2013.

[14] H. Choset, "Coverage for robotics–a survey of recent results," *Annals of Mathematics and Artificial Intelligence*, vol. 31, pp. 113–126, 2001.

[15] E. U. Acar, H. Choset, A. A. Rizzi, P. N. Atkar, and D. Hull, "Morse decompositions for coverage tasks," *International Journal of Robotics Research*, vol. 21, no. 4, pp. 331–344, 2002.

[16] S. Hert, S. Tiwari, and V. Lumelsky, "A terrain-covering algorithm for an auv," *Autonomous Robots*, vol. 3, pp. 91–119, 1996.

[17] P. Cheng, J. Keller, and V. Kumar, "Time-optimal uav trajectory planning for 3d urban structure coverage," in *Intelligent Robots and Systems, 2008. IROS 2008. IEEE/RSJ International Conference on*, sept. 2008, pp. 2750 –2757.

[18] T.-S. Lee, J.-S. Choi, J.-H. Lee, and B.-H. Lee, "3-d terrain covering and map building algorithm for an auv," in *Proc. IEEE/RSJ Int. Conf. Intelligent Robots and Systems IROS 2009*, 2009, pp. 4420–4425.

[19] P. N. Atkar, H. Choset, A. A. Rizzi, and E. U. Acar, "Exact cellular decomposition of closed orientable surfaces embedded in r3," in *Proc. Int. Conf. Robotics and Automation*, vol. 1, 2001, pp. 699–704.

[20] P. Atkar, A. L. Greenfield, D. C. Conner, H. Choset, and A. Rizzi, "Uniform coverage of automotive surface patches," *The International Journal of Robotics Research*, vol. 24, no. 11, pp. 883 – 898, November 2005.

[21] T. Oksanen and A. Visala, "Coverage path planning algorithms for agricultural field machines," *Journal of Field Robotics*, vol. 26, no. 8, pp. 651–668, 2009.

[22] A. Xu, P. Virie, and I. Rekleitis, "Optimal complete terrain coverage using an unmanned aerial vehicle," in *Proceedings of the 2011 IEEE International Conference on Robotics & Automation*, 2011.

[23] A. Barrientos, J. Colorado, J. del Cerro, A. Martinez, C. Rossi, D. Sanz, and J. Valente, "Aerial remote sensing in agriculture: A practical approach to area coverage and path planning for fleets of mini aerial robots," *Journal of Field Robotics*, vol. 28, no. 5, pp. 667–689, 2011.

[24] S. Guo and B. Gao, "Path-planning optimization of underwater microrobots in 3-d space by pso approach," in *Robotics and Biomimetics (ROBIO), 2009 IEEE International Conference on*, dec. 2009, pp. 1655 –1620.

[25] J. Carsten, D. Ferguson, and A. Stentz, "3d field d: Improved path planning and replanning in three dimensions," in *Intelligent Robots and Systems, 2006 IEEE/RSJ International Conference on*, oct. 2006, pp. 3381 –3386.

[26] B. Englot and F. Hover, "Sampling-based coverage path planning for inspection of complex structures," in *International Conference on Automated Planning and Scheduling (ICAPS)*, 2012.

[27] J. Poppinga, A. Birk, K. Pathak, and N. Vaskevicius, "Fast 6-dof path planning for autonomous underwater vehicles (auv) based on 3d plane mapping," in *Safety, Security, and Rescue Robotics (SSRR), 2011 IEEE International Symposium on*, nov. 2011, pp. 345 –350.

[28] A. Hornung, K. Wurm, M. Bennewitz, C. Stachniss, and W. Burgard, "Octomap: an efficient probabilistic 3d mapping framework based on octrees," *Autonomous Robots*, vol. 34, no. 3, pp. 189–206, 2013.

[29] R. H. Bartels, J. C. Beatty, and B. A. Barsky, *An Introduction to Splines for Use in Computer Graphics &Amp; Geometric Modeling*. San Francisco, CA, USA: Morgan Kaufmann Publishers Inc., 1987.

[30] E. Galceran and M. Carreras, "Planning coverage paths on bathymetric maps for in-detail inspection of the ocean floor," in *Proc. In-*

ternational Conference on Robotics and Automation, 2013.
[31] D. Ribas, N. Palomeras, P. Ridao, M. Carreras, and A. Mallios, "Girona 500 auv, from survey to intervention," *IEEE/ASME Transactions on Mechatronics*, vol. 17, no. 1, pp. 46–53, 2012.
[32] N. Palomeras, A. El-Fakdi, M. Carreras, and P. Ridao, "Cola2: A control architecture for auvs," *Oceanic Engineering, IEEE Journal of*, vol. 37, no. 4, pp. 695–716, 2012.
[33] M. Prats, J. Perez, J. Fernandez, and P. Sanz, "An open source tool for simulation and supervision of underwater intervention missions," in *Intelligent Robots and Systems (IROS), 2012 IEEE/RSJ International Conference on*, 2012, pp. 2577–2582.